ChemComm

COMMUNICATION

View Article Online
View Journal | View Issue

Cite this: *Chem. Commun.*, 2017, 53, 2142

Received 21st December 2016,
Accepted 24th January 2017

DOI: 10.1039/c6cc10145c

rsc.li/chemcomm

Surface-selective direct ^{17}O DNP NMR of CeO_2 nanoparticles†

Michael A. Hope,[a] David M. Halat,[a] Pieter C. M. M. Magusin,[a] Subhradip Paul,[b] Luming Peng[c] and Clare P. Grey*[a]

Surface-selective direct ^{17}O DNP has been demonstrated for the first time on CeO_2 nanoparticles, for which the first three layers can be distinguished with high selectivity. Polarisation build-up curves show that the polarisation of the (sub-)surface sites builds up faster than the bulk, accounting for the remarkable surface selectivity.

Nanoparticulate transition metal oxides are of technological importance in various areas of chemistry and materials science, such as catalysis, energy storage and electronics.[1–4] However, optimisation of materials for these applications necessitates thorough knowledge of structure–function relationships, which in turn requires an accurate description of the local surface structure. In catalytic processes, oxygen at or near the surface of *e.g.* CeO_2 nanoparticles is believed to constitute (part of) the catalytically active sites,[5] yet the identity and role of specific surface oxide environments in this and other nanoparticle systems remains uncertain.

Nuclear magnetic resonance (NMR) spectroscopy can reveal a wealth of chemical and structural information on the atomic scale, and previous work has shown that ^{17}O solid-state NMR (ssNMR) spectroscopy is a powerful tool in investigating the structure and activity of zeolites,[6] metal oxide nanoparticles,[7,8] and other functionally relevant oxides.[9] However, the inherent difficulty of attaining sufficient signal to noise in NMR spectroscopy is exacerbated for experiments on ^{17}O, the only NMR-active nucleus of oxygen, as its low natural abundance (0.037%) leads to lower intensity and its quadrupolar character ($I = 5/2$) can result in additional spectral broadening.

The challenges of acquiring ssNMR spectra are further confounded when studying surface environments, as they typically constitute a small fraction of the sample. Nonetheless, in recent work by Wang *et al.*, ^{17}O ssNMR spectra of nanoparticulate CeO_2 have been recorded and assigned to specific surface environments *via* a combination of surface-selective enrichment (with $H_2{}^{17}O$) and density functional theory (DFT) calculations.[8] However, in this case the surface-selective enrichment is only possible due to the high reactivity of ceria.

A more general approach to overcome the sensitivity problems inherent to ssNMR is the use of dynamic nuclear polarisation (DNP),[10] which has seen a significant resurgence in recent years. In a typical DNP experiment, the sample is impregnated with radicals in a frozen glassy solvent, and the spin polarisation of the unpaired electrons on the radicals is transferred to the NMR-active nuclei *via* application of high-frequency microwave radiation. As the equilibrium polarisation of the electron is much greater than that of nuclei, NMR signal enhancements exceeding a factor of 200 have been achieved.[11]

DNP can be applied in two ways: in direct DNP, the nucleus of interest is directly polarised by the radicals, whereas in indirect DNP, ^1H nuclei are first polarised and cross polarisation (CP) is then used to transfer the ^1H polarisation to the nucleus of interest. The latter approach typically leads to larger enhancement factors and permits shorter recycle delays, but requires ^1H nuclei embedded in the sample. In particular, indirect DNP has been used to record the ^{13}C NMR spectra of surface organic species covalently incorporated into silica frameworks,[12] the ^{17}O NMR spectra of surface hydroxyl groups in mesoporous silica nanoparticle samples[13] and the ^{27}Al NMR spectra of surface sites in γ-alumina nanoparticles.[14] Direct DNP has been used to record the ^{27}Al NMR spectra of surface sites in mesoporous alumina–silica[15] and the ^{17}O NMR spectra of MgO.[16] However, to our knowledge, direct DNP has not thus far been used to perform surface-sensitive ^{17}O ssNMR spectroscopy.

In this work, CeO_2 nanoparticles are investigated in order to establish the feasibility of surface-selective direct DNP ^{17}O NMR. The CeO_2 nanoparticles (Sigma Aldrich) were first

[a] *Department of Chemistry, University of Cambridge, Lensfield Road, Cambridge, CB2 1EW, UK. E-mail: cpg27@cam.ac.uk*
[b] *DNP MAS NMR Facility, Sir Peter Mansfield Magnetic Resonance Centre, University of Nottingham, Nottingham, NG7 2RD, UK*
[c] *Key Laboratory of Mesoscopic Chemistry of MOE, School of Chemistry and Chemical Engineering, Nanjing University, Nanjing, 210093, China*

† Electronic supplementary information (ESI) available: Experimental details, conventional ssNMR spectra, fitting of the sidebands, the effect of air exposure, DNP build-up curve analysis, comparison with CeO_2 nanorods and the effect of a field sweep on the DNP enhancement. See DOI: 10.1039/c6cc10145c

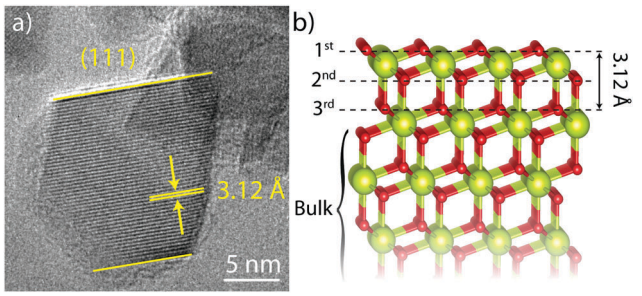

Fig. 1 (a) HRTEM image of a CeO_2 nanoparticle showing (111) fringes, (111) surfaces and an octahedral morphology (in projection), and (b) the structure of a (111) O-terminated CeO_2 surface showing the first three oxygen layers and the (111) spacing. Cerium atoms are larger and yellow while oxygen atoms are smaller and red.

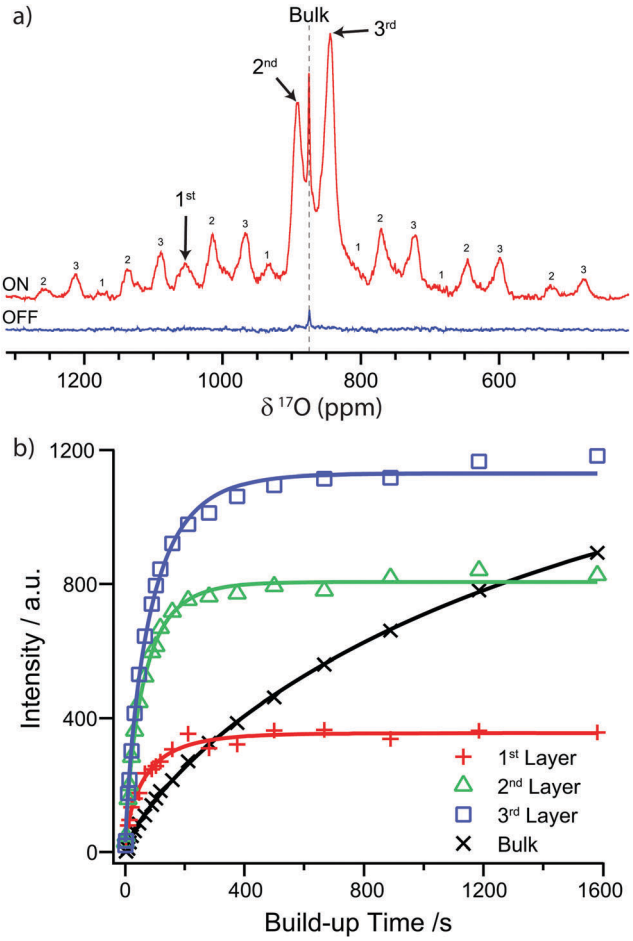

Fig. 2 (a) ^{17}O NMR (14.1 T) spectra of ^{17}O enriched CeO_2 nanoparticles mixed with the TEKPol radical in TCE, with and without microwave irradiation, using a presaturated Hahn echo experiment. The spectra were recorded at 95 K. The OFF spectrum was recorded at 12.5 kHz MAS, whereas the ON spectrum was recorded at 10 kHz in order to separate the spinning sidebands from the signal arising from the first layer. Spinning sidebands are labelled according to the layer of the signal from which they arise. (b) The ^{17}O saturation recovery build-up curves for the different environments in CeO_2 nanoparticles and the fitted stretched exponentials. The intensity is determined by deconvoluting the isotropic peaks (see Fig. S8 and discussion in ESI†).

investigated using transmission electron microscopy (TEM) (Fig. 1a); this showed a predominantly octahedral morphology with an average particle size of 11 ± 5 nm. Identification of the (111) fringes with a spacing of 3.12 Å revealed that the particles were dominated by (111) facets, the structure of which is shown in Fig. 1b.

The nanoparticles were then enriched with $^{17}O_2$ (Cambridge Isotope Laboratories) at 350 °C for 24 hours and subsequently handled under an inert atmosphere (Ar or N_2 gloveboxes) as the first surface layer readily exchanges with oxygen in the air, leading to loss of enrichment. TEM analysis of the enriched samples revealed minor coarsening with a subsequent average particle size of 15 ± 3 nm. To perform DNP experiments, the nanoparticles were wetted with the TEKPol biradical[11] in 1,1,2,2-tetrachloroethane (TCE), and packed into a 3.2 mm sapphire rotor. This combination has been chosen rather than the alternative AMUPol/H_2O,[17] as the presence of un-enriched water can lead to removal of ^{17}O from the first layer.[8,18] ^{17}O DNP NMR spectra were then recorded at 14.1 T under low temperature (~95 K) magic angle spinning (MAS) using a pre-saturated Hahn-echo experiment, with a single rotor echo delay (100 μs). Fig. 2a shows the ^{17}O ssNMR spectra recorded with and without microwave irradiation ("ON" and "OFF" respectively), with 8 scans and a recycle delay of 60 s. Without microwave irradiation, only the sharp signal due to the single bulk oxygen environment could be observed, whereas under microwave irradiation three new features were distinguished; these are ascribed to (sub-)surface sites selectively enhanced by TEKPol radicals in the vicinity of the surface.

By comparison with the DFT calculations of Wang *et al.*,[8] these features at 1055, 893, and 843 ppm are identified as oxygen sites within the first, second and third (sub-)surface layers, respectively (labelled in Fig. 1b). There is some discrepancy between the chemical shifts observed in this work and those reported by Wang *et al.*, which is ascribed to minor differences between the CeO_2 samples (see Table S1 and discussion in ESI†). The (sub-)surface sites also have a larger anisotropy than the bulk as evidenced by the greater intensity of their spinning sideband manifolds, consistent with the reduction of symmetry at the surface. The DFT calculations suggest that the sideband intensity predominately arises from satellite transitions which are broadened by the larger quadrupolar coupling constants (C_Q) of the (sub-)surface sites (100–135 kHz for the first three layers *cf.* zero for the tetrahedral bulk sites); however, this alone does not fully account for the sideband intensity. Another contributing factor is the electron–nuclear dipolar coupling with the radicals; however, simulation of the sideband manifold suggests that bulk magnetic susceptibility effects due to the paramagnetic matrix[19] must dominate (see Fig. S3 and discussion in ESI†). The origin of the broadening of the (sub-)surface signals observed with DNP can be identified by comparing the DNP spectrum to the conventional room temperature ssNMR spectra, with and without the addition of radicals (Fig. S5 and S1 respectively, ESI†), which shows that the broadness is caused by freezing out of motional averaging at ~95 K, most likely of the radicals.

The observed surface selectivity in direct DNP occurs because the radicals are external to the particles and the rate of polarisation transfer from the radical to a nucleus falls off rapidly (as $1/r^6$).[20] Nuclei at the surface can therefore be hyperpolarised by the radicals, but for sites within the deeper subsurface layers, the excess nuclear spin polarisation must travel *via* spin diffusion, which is thought to be slow for ^{17}O (in part due to the low natural abundance and gyromagnetic ratio),[21] leading to a longer build-up time.

To test this hypothesis, the DNP build-up time constant (T_{DNP}) was determined for each feature using a saturation recovery experiment (see ESI† for further details). The nuclear magnetisation was first nullified with a saturation pulse train and then allowed to build up *via* DNP for a variable time before measuring the resulting magnetisation by recording the ^{17}O NMR spectrum. The build-up time was found by fitting the signal intensity to a stretched exponential function of the form

$$I = I_0\left(1 - \exp\left[-\left(\frac{t}{T_{DNP}}\right)^{\beta}\right]\right),$$

with I_0 the maximum signal intensity and $\beta < 1$ the stretching exponent. A stretched exponential function describes a build-up process consisting of a distribution of time constants characterised by T_{DNP}; a smaller β parameter indicates a broader distribution.[22] The build-up curves are shown in Fig. 2b, with fitted time constants T_{DNP} in Table 1. The bulk site exhibits a slow build-up (continuing beyond the maximum recorded time of 1600 s), as spin polarisation must diffuse a significant distance. In contrast, T_{DNP} of the (sub-)surface sites is much shorter, accounting for the observed surface selectivity. The maximum signal intensity of the (sub-)surface sites is given by a combination of the enrichment level, the DNP enhancement and the degree of quenching (loss of signal due to broadening and extremely fast nuclear relaxation very near the radicals).[23] The conventional ssNMR spectrum recorded without radicals shows that the enrichment of the first three (sub-)surface layers is approximately equal (Fig. S1 and Table S2, ESI†); the differences observed in the maximum signal intensity therefore show that the first layer is quenched more than the second layer, which in turn is quenched more than the third layer, due to closer proximity to the radicals, and that the greater degree of quenching outweighs any increase in DNP enhancement.

A second experiment has been performed on a sample of the same nanoparticles, but enriched with a higher pressure of $^{17}O_2$ and stored under ambient conditions (Fig. S4, ESI†). For this sample, the second and third layer sites are again observed but the signal arising from the first layer is not observed due to exchange with $^{16}O_2$ in air; this can be shown by re-recording the conventional ssNMR spectrum after progressive exposure to air and observing the concomitant reduction in signal for the first layer (Fig. S7, ESI†). The bulk signal is more intense than previously, which is ascribed to increased incorporation of ^{17}O due to the larger $^{17}O_2$ pressure during enrichment; the build-up time constant for the bulk signal is also smaller than the previous sample (T_{DNP} = 586 s, Fig. S6, ESI†), which is ascribed to faster spin diffusion into the bulk due to the greater enrichment, because spin diffusion is strongly dependent on the concentration of the spin-active nucleus. The higher enrichment level also allows the (sub-)surface sites to be observed without DNP in a long (12 h) experiment (Fig. S5, ESI†), and hence DNP enhancements ($\varepsilon_{ON/OFF}$) for the second and third layers can be measured as 56 and 29, respectively. The larger enhancement of the second layer is presumably due to less efficient hyperpolarisation of the more distant third layer (the quenching due to radicals is present with or without microwave irradiation, so does not affect the enhancement factor). The bulk site exhibits only a very minor enhancement as it is dominated by atoms far from the surface which are not hyperpolarised. We note, however, that as a recycle delay of 60 s is insufficient to obtain the maximum signal either with or without microwave irradiation, the observed enhancement factors for all sites will be dependent on the recycle delay. As has been previously addressed by Lee *et al.*, $\varepsilon_{ON/OFF}$ should be seen as a guide to the DNP enhancement rather than a fundamental parameter.[23] These results show that the DNP NMR spectra of CeO_2 nanoparticles are sensitive to details of sample preparation, which can in turn give insight into the mechanisms of DNP.

To compare with these direct DNP experiments, indirect DNP ($^1H \rightarrow {}^{17}O$) NMR spectra were also recorded on the first nanoparticulate CeO_2 sample (Fig. 3). These revealed ^{17}O signals centred at 225 ppm and −20 ppm, which are ascribed to Ce–OH terminations and H_2O molecules adsorbed to the

Table 1 The fitted direct DNP build-up time constants for the different ^{17}O environments in CeO_2 nanoparticles

	Bulk	1st Layer	2nd Layer	3rd Layer
Shift/ ppm	875	1055	893	843
T_{DNP} /s	>1600	67 ± 6	62 ± 2	85 ± 3

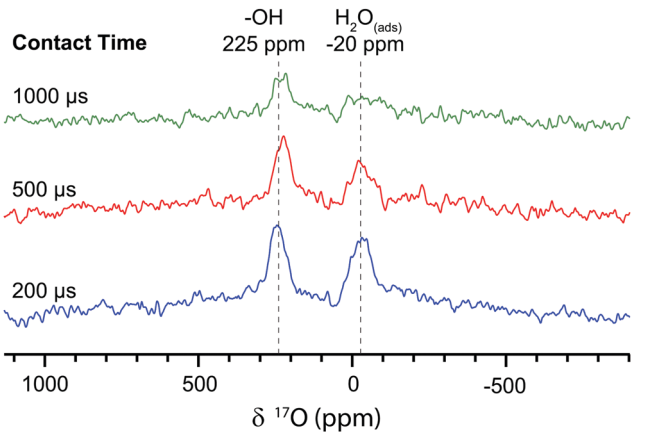

Fig. 3 The indirect DNP ^{17}O NMR (14.1 T) spectra of ^{17}O enriched CeO_2 nanoparticles impregnated with TEKPol in TCE, recorded at 12.5 kHz MAS with a recycle delay of 4.3 s, 320 scans and variable contact times for the $^1H \rightarrow {}^{17}O$ cross polarisation. The ^{17}O magnetisation was pre-saturated to avoid the direct DNP signal.

surface, respectively, again in agreement with Wang *et al.*[8] These assignments are supported by the short CP contact time of 200 μs required to attain the maximum CP intensity, which is indicative of direct O–H bonding; the signal is attenuated with longer contact times. These signals could not be observed with direct DNP, even when the carrier frequency was varied and the field was swept to optimise the enhancements (Fig. S10, ESI†), but require the greater enhancement factors achievable with indirect DNP. The indirect DNP experiments do not, however, exhibit evidence for the (sub-)surface sites identified *via* direct DNP NMR, even under conditions of longer contact times and variable rf carrier frequencies (efficient CP is only observed to signals close to the carrier frequency). The lack of (sub-)surface oxygen features is attributed to the $1/r^6$ dependence of CP on distance and the difficulty of spin-locking the quadrupolar ^{17}O nucleus, so that only oxygen atoms directly bonded to hydrogen can be readily seen.[24] Furthermore, there are few hydroxyl terminations and adsorbed water molecules on surfaces of CeO_2 samples oxidised at >300 °C,[25] and the hydrophobic TCE solvent does not adsorb strongly, so insufficient protons exist in the vicinity of the surface to permit efficient CP. Therefore, direct DNP is needed in this case to observe surface and sub-surface oxygen sites in nanoparticulate CeO_2.

Finally, to determine whether (sub-)surface signals could be used to distinguish between differing morphologies, CeO_2 nanorods were also investigated by direct ^{17}O DNP NMR (ESI,† Section 8); surface selectivity was again observed with a reduction in the intensity of the second sub-surface layer, which may indicate preferential segregation of oxygen vacancies.

In conclusion, surface-selective direct ^{17}O DNP NMR spectroscopy has been demonstrated for the first time, using a system of CeO_2 nanoparticles, for which the first three layers can be distinguished with high selectivity. This selectivity is ascribed to the slow spin diffusion of ^{17}O polarisation into the bulk, so that only the (sub-)surface sites are efficiently hyper-polarised by radicals in the vicinity of the surface. This is corroborated by the build-up curves for the different signals and by comparison between samples with different degrees of enrichment. It is shown that although indirect DNP can be used to identify –OH terminations and adsorbed water on the CeO_2 surface, it is not possible to observe the aforementioned (sub-)surface sites *via* this approach due to the scarcity of protons near the surface and the difficulty of long-distance $^1H \rightarrow {}^{17}O$ cross polarisation; (sub-)surface sites can only be detected with direct DNP. The observed (sub-)surface signals can be used to distinguish between morphologies and we note that this approach may be extended to other systems where protons are not available to allow indirect DNP experiments, or where the surfaces are sensitive to water exposure.

We are grateful for financial support by the Oppenheimer Foundation (M. A. H.), the Cambridge Commonwealth Trusts (D. M. H.), the National Natural Science Foundation of China (NSFC) (21573103 and 21661130149) and the Royal Society Newton Fund (L. P.). The DNP experiments were performed at the DNP MAS NMR Facility at the University of Nottingham, with thanks to the EPSRC for funding of pilot studies (EP/L022524/1). We would also like to thank Dr D. A. Jefferson (Cambridge) for acquiring the TEM images and for useful discussions, Craig Stoppiello and Prof. A. N. Khlobystov (Nottingham) for use of their glovebox, Dr Xin-Ping Wu and Dr Xue-Qing Gong (ECUST, Shanghai) for the DFT calculations on CeO_2 and Dr Yuxian Gao and Prof. Weixin Huang (University of Science and Technology of China) for synthesising the CeO_2 nanorods. The experimental data for all NMR experiments have been made available at DOI: 10.17863/CAM.7267.

References

1 M. Fernández-García and J. A. Rodriguez, in *Encyclopedia of Inorganic and Bioinorganic Chemistry*, John Wiley & Sons, 2011.
2 Y. Ren, Z. Liu, F. Pourpoint, A. R. Armstrong, C. P. Grey and P. G. Bruce, *Angew. Chem., Int. Ed.*, 2012, **51**, 2164–2167.
3 P. Poizot, S. Laruelle, S. Grugeon, L. Dupont and J.-M. Tarascon, *Nature*, 2000, **407**, 496–499.
4 M. S. Chen and D. W. Goodman, *Science*, 2004, **306**, 252–255.
5 Q. Fu, H. Saltsburg and M. Flytzani-Stephanopoulos, *Science*, 2003, **301**, 935–938.
6 L. Peng, Y. Liu, N. Kim, J. E. Readman and C. P. Grey, *Nat. Mater.*, 2005, **4**, 216–219.
7 E. Scolan, C. Magnenet, D. Massiot and C. Sanchez, *J. Mater. Chem.*, 1999, **9**, 2467–2474.
8 M. Wang, X.-P. Wu, S. Zheng, L. Zhao, L. Li, L. Shen, Y. Gao, N. Xue, X. Guo, W. Huang, Z. Gan, F. Blanc, Z. Yu, X. Ke, W. Ding, X.-Q. Gong, C. P. Grey and L. Peng, *Sci. Adv.*, 2015, **1**, e1400133.
9 D. M. Halat, R. Dervişoğlu, G. Kim, M. T. Dunstan, F. Blanc, D. S. Middlemiss and C. P. Grey, *J. Am. Chem. Soc.*, 2016, **138**, 11958–11969.
10 Q. Z. Ni, E. Daviso, T. V. Can, E. Markhasin, S. K. Jawla, T. M. Swager, R. J. Temkin, J. Herzfeld and R. G. Griffin, *Acc. Chem. Res.*, 2013, **46**, 1933–1941.
11 A. Zagdoun, G. Casano, O. Ouari, M. Schwarzwälder, A. J. Rossini, F. Aussenac, M. Yulikov, G. Jeschke, C. Coperet, A. Lesage, P. Tordo and L. Emsley, *J. Am. Chem. Soc.*, 2013, **135**, 12790–12797.
12 A. Lesage, M. Lelli, D. Gajan, M. A. Caporini, V. Vitzthum, P. Miéville, J. Alauzun, A. Roussey, C. Thieuleux, A. Mehdi, G. Bodenhausen, C. Copéret and L. Emsley, *J. Am. Chem. Soc.*, 2010, **132**, 15459–15461.
13 F. A. Perras, U. Chaudhary, I. I. Slowing and M. Pruski, *J. Phys. Chem. C*, 2016, **120**, 11535–11544.
14 V. Vitzthum, P. Miéville, D. Carnevale, M. A. Caporini, D. Gajan, C. Copéret, M. Lelli, A. Zagdoun, A. J. Rossini, A. Lesage, L. Emsley and G. Bodenhausen, *Chem. Commun.*, 2012, **48**, 1988.
15 A. Lund, M.-F. Hsieh, T.-A. Siaw and S.-I. Han, *Phys. Chem. Chem. Phys.*, 2015, **17**, 25449–25454.
16 F. Blanc, L. Sperrin, D. A. Jefferson, S. Pawsey, M. Rosay and C. P. Grey, *J. Am. Chem. Soc.*, 2013, **135**, 2975–2978.
17 C. Sauvée, M. Rosay, G. Casano, F. Aussenac, R. T. Weber, O. Ouari and P. Tordo, *Angew. Chem., Int. Ed.*, 2013, **52**, 10858–10861.
18 Y. Champouret, Y. Coppel and M. L. Kahn, *J. Am. Chem. Soc.*, 2016, **138**, 16322–16328.
19 A. S. L. Thankamony, O. Lafon, X. Lu, F. Aussenac, M. Rosay, J. Trébosc, H. Vezin and J. P. Amoureux, *Appl. Magn. Reson.*, 2012, **43**, 237–250.
20 K. R. Thurber and R. Tycko, *J. Chem. Phys.*, 2012, **137**, 84508.
21 F. A. Perras, T. Kobayashi and M. Pruski, *J. Am. Chem. Soc.*, 2015, **137**, 8336–8339.
22 L. Holmes, L. Peng, I. Heinmaa, L. A. O;Dell, M. E. Smith, R.-N. Vannier and C. P. Grey, *Chem. Mater.*, 2008, **20**, 3638–3648.
23 D. Lee, S. Hediger and G. De Paëpe, *Solid State Nucl. Magn. Reson.*, 2015, **66**, 6–20.
24 J. P. Amoureux and M. Pruski, *Mol. Phys.*, 2002, **100**, 1595–1613.
25 A. Laachir, V. Perrichon, A. Badri, J. Lamotte, E. Catherine, J. C. Lavalley, J. El Fallah, L. Hilaire, F. Le Normand, E. Quéméré, G. N. Sauvion and O. Touret, *J. Chem. Soc., Faraday Trans.*, 1991, **87**, 1601–1609.